Koc. J. Sci. Eng., 2026(17): 136-143 https://doi.org/10.34088/kojose.1860665

Kocaeli University

Kocaeli Journal of Science and Engineering

http://dergipark.org.tr/kojose

Modified Nodal Analysis of Zero Current Switching Resonant Push-Pull Converter

Yusuf Can AYDIN [1,*], Ali Bekir YILDIZ [2]

[1] *Department of Electrical Engineering, Kocaeli University, Kocaeli, Türkiye,* ***ORCID:*** *0009-0006-8401-5489*
[2] *Department of Electrical Engineering, Kocaeli University, Kocaeli, Türkiye,* ***ORCID:*** *0000-0003-4043-7859*

Article Info

Research paper

Received : *January 10, 2026*
Accepted : *April 29, 2026*

Abstract

In this study, a conventional hard-switching push-pull DC–DC converter topology is transformed into a resonant converter by employing a soft-switching technique. The governing circuit equations of the resulting resonant topology are systematically derived. An analytical model based on Modified Nodal Analysis (MNA) is developed to investigate the performance of the proposed soft-switching push-pull converter. Unlike the conventional push-pull configuration, the integration of a resonant tank enables Zero Current Switching (ZCS), which significantly reduces the thermal load and current stress on the semiconductor devices.

Keywords

LC Tank
Modified Nodal Analysis
Push-Pull Converter
Resonance Converter
Zero-Current Switching

1. Introduction

Power electronics applications today span a wide range of fields, from renewable energy systems to electric vehicles. The fundamental performance requirements expected from power electronic systems include high efficiency, low switching losses, reduced electromagnetic interference (EMI) levels, and high-power density[1,2]. In conventional hard switching systems, the switching losses generated during operation and the resulting thermal stress constitute a significant challenge[3].

To overcome these challenges, soft-switching techniques have been widely adopted. Zero-current switching (ZCS) and zero-voltage switching (ZVS) techniques significantly reduce switching losses[4,5]. Various resonant circuit topologies are preferred based on distinct application areas and cost requirements. All these configurations are designed to decrease switching losses[6]. High-frequency switching is essential for reducing the physical dimensions of winding components—such as transformers and inductors—and minimizing overall circuit footprints. However, in hard-switching topologies, increasing the frequency results in a proportional escalation of switching losses. By designing zero current switching (ZCS) techniques within a similar circuit topology, the adverse effects induced by high-frequency operation can be effectively reduced[7].

In this context, resonant converters enable soft switching by shaping circuit currents and voltages into sinusoidal waveforms using an LC resonant network[8].

The push-pull converter is a preferred topology for medium- and high-power applications due to its isolated structure and symmetric power transfer capability. The push-pull configuration is a highly suitable topology for boost applications, because of its inherent high voltage gain capability[9]. Owing to its energy transfer mechanism, it exhibits similarities to flyback converters; however, the continuous nature of power transfer renders the push-pull topology more advantageous[10,11]. In conventional push-pull converters, recovery losses and EMI issues-particularly arising from hard switching of the output diodes-represent notable drawbacks[12].

* Corresponding Author: ayusufcan06@gmail.com

Consequently, in recent years, the integration of an LC resonant tank into conventional push-pull converters has attracted considerable attention, as it enables zero-current switching of both diodes and switching devices[13]. This approach effectively mitigates switching losses and EMI-related issues[14].

The analytical investigation of such complex resonant structures becomes challenging when using conventional analysis methods. This difficulty can be effectively addressed by employing Modified Nodal Analysis (MNA). MNA is a powerful matrix-based circuit analysis technique that allows all circuit elements and switching states to be systematically modeled[15,16]. Modified Nodal Analysis (MNA) is a method employed to solve differential equations and obtain waveforms of nodes derived through Kirchhoff's laws[17]. MNA is flexible, and packaged software for circuit analysis uses MNA[18].

The push-pull converter is inherently a two-switch topology. Due to the growing demand for high-efficiency power converters, many converter topologies have undergone various structural modifications. In particular, the performance differences between hard and soft-switching techniques have led engineers to increasingly favor soft-switching approaches[19]. Various methods have been proposed to modify converter topologies to achieve soft-switching operation. Ultimately, the resonant behavior produced by square-wave excitation applied to an LC resonant tank forms the fundamental basis of soft switching[20].

The remainder of this paper is organized as follows. Section 2 presents the structure of the conventional push-pull converter and subsequently introduces the LC resonant tank integration. The MNA-based system equations and simulation results are provided in Section 3. Finally, the study is concluded in Section 4.

2. ZCS Push-Pull Topology

In the conventional push-pull circuit shown in Fig. 1, the system does not include any structure capable of producing resonant behavior. The output diodes operate under hard switching conditions. Due to hard switching, electromagnetic interference (EMI) and switching losses become significant issues; therefore, various snubber circuits are commonly employed at the output diodes to suppress these adverse effects.

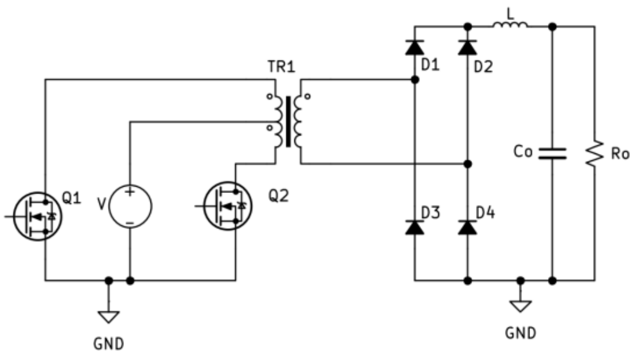

Figure 1. Conventional Push-Pull Converter Circuit

In the zero-current switching (ZCS) push-pull topology, no modifications are introduced on the primary side of the converter. On the secondary side, the interaction between the square-wave voltage generated by the transformer secondary windings and the LC network results in the formation of sinusoidal waveforms. These sinusoidal waveforms enable softer switching behavior by providing zero-crossing conditions, thereby preventing abrupt current and voltage transients across the output diodes.

2.1. ZCS Push-Pull Resonant Circuit

Compared with the conventional topology, the ZCS push-pull converter incorporates an additional capacitor and inductor, forming an LC resonant tank[16]. The circuit schematic is illustrated in Fig. 2. The sinusoidal waveforms generated within this LC resonant tank facilitate zero-current switching operation.

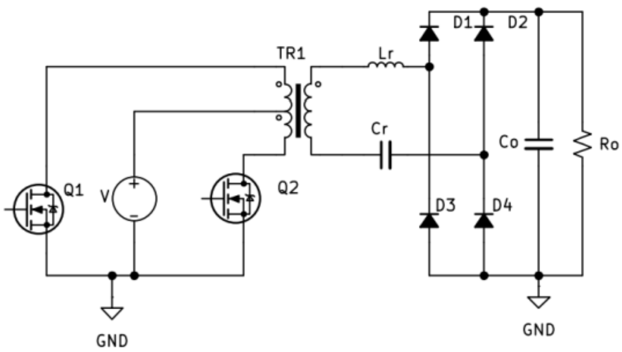

Figure 2. Resonance Push-Pull Converter Circuit

2.2. LC Resonant Tank Design

The inductor and capacitor responsible for generating resonance constitute the LC resonant tank. Since the operation of this tank circuit is inherently frequency-dependent, the design process begins with the selection of the operating frequency.

$$f_r = \frac{1}{2\pi\sqrt{LC}} \tag{1}$$

As expressed in Equation 1, the resonant components must be selected according to the predetermined switching frequency of the transducer to ensure proper resonant operation.

3. MNA-Based Circuit Analysis

Modified Nodal Analysis (MNA) is a circuit analysis technique based on Kirchhoff's current law. In this method, all circuit nodes, elements, and sources are formulated into a matrix-based system of equations and solved simultaneously, as expressed in Equation 2.

$$GX_{(t)} + C\frac{dX}{dt} = BU_{(t)} \tag{2}$$

The G matrix is constructed from frequency-independent elements, whereas the C matrix consists of frequency-dependent energy storage components, including inductors and capacitors. The X matrix represents the vector of unknown node voltages and branch currents to be solved within the MNA framework. Before solving the circuit equations, the primary side of the transformer is referred to the secondary side to simplify the analysis. By applying this transformation, the explicit modeling of the transformer is omitted. Consequently, the 50V square-wave voltage at the primary side is scaled by the turn ratio n, yielding a 500V waveform on the secondary side. The equivalent circuit obtained after this transformation is illustrated in Fig. 3.

Given the leakage inductances on the primary and secondary sides of the designed push-pull transformer, the primary leakage inductance is significantly smaller than the secondary leakage inductance and can be neglected. As is common in many transformer-based resonant circuits, the leakage inductance of the transformer is used as a part of the resonant tank. Specifically, the secondary leakage inductance L_{lks} functions as the resonant inductance L_r defined in the design, while L_{eq} represents the magnetizing inductance of the transformer.

The inductor L_{eq} represents the magnetizing inductance reflected to the primary side and models the magnetic energy storage of the transformer. It is included to ensure the accuracy of the MNA analysis. Since its value is sufficiently large, it does not significantly affect the resonant behavior of the circuit.

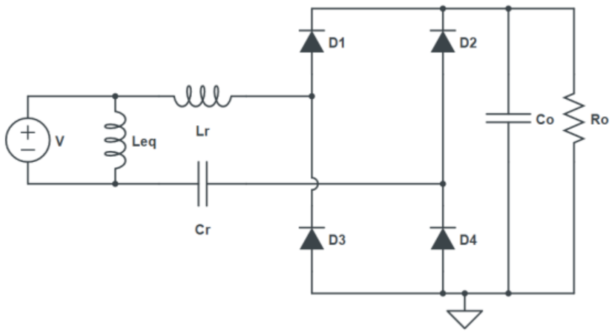

Figure 3. Simplified Secondary Circuit

For modelling the switching devices, a two-valued resistance approach is employed. Accordingly, the switches are represented by a minimum resistance in the ON state and a maximum resistance in the OFF state, as illustrated in Fig. 4. This approach enables efficient incorporation of switching behavior into the MNA formulation. By using this two-valued resistance model, computations can be performed without requiring any modifications to the fundamental system equations.

The series resistance R_{ser}, connected in series with the voltage source, represents the internal resistance of the supply. This resistance is introduced to avoid directly connecting energy storage elements, such as inductors and capacitors, in parallel with ideal voltage sources, thereby improving numerical stability and yielding more realistic simulation results.

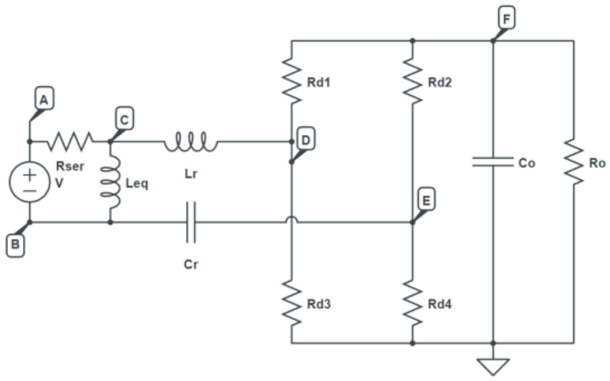

Figure 4. MNA Circuit

Using the MNA method, the matrices G, B, C, and the state vector X_n are derived from the circuit schematics and presented Equations 3, 4, 5 and 6. These matrices comprehensively describe the dynamic behavior of the proposed resonant push-pull converter.

$$\mathbf{C}=\begin{bmatrix} 0 & 0 & 0 & 0 & 0 & 0 & 0 & 0 & 0 \\ 0 & C_r & 0 & 0 & -C_r & 0 & 0 & 0 & 0 \\ 0 & 0 & 0 & 0 & 0 & 0 & 0 & 0 & 0 \\ 0 & 0 & 0 & 0 & 0 & 0 & 0 & 0 & 0 \\ 0 & -C_r & 0 & 0 & C_r & 0 & 0 & 0 & 0 \\ 0 & 0 & 0 & 0 & 0 & C_o & 0 & 0 & 0 \\ 0 & 0 & 0 & 0 & 0 & 0 & -L_m & 0 & 0 \\ 0 & 0 & 0 & 0 & 0 & 0 & 0 & -L_r & 0 \\ 0 & 0 & 0 & 0 & 0 & 0 & 0 & 0 & 0 \end{bmatrix} \quad (3)$$

$$\boldsymbol{B} = [0 \quad 0 \quad 0 \quad 0 \quad 0 \quad 0 \quad 0 \quad 0 \quad 1]^T \quad (4)$$

$$\boldsymbol{X_n} = \begin{bmatrix} V_A & V_B & V_C & V_D & V_E & V_F & I_{L_r} & I_{L_{eq}} & I_E \end{bmatrix}^T \quad (5)$$

$$\mathbf{G}=\begin{bmatrix} \frac{1}{R_{ser}} & 0 & -\frac{1}{R_{ser}} & 0 & 0 & 0 & 0 & 0 & 1 \\ 0 & 0 & 0 & 0 & 0 & 0 & -1 & 0 & -1 \\ -\frac{1}{R_{ser}} & 0 & \frac{1}{R_{ser}} & 0 & 0 & 0 & 1 & 1 & 0 \\ 0 & 0 & 0 & \frac{1}{R_{d1}}+\frac{1}{R_{d3}} & 0 & -\frac{1}{R_{d1}} & 0 & -1 & 0 \\ 0 & 0 & 0 & 0 & \frac{1}{R_{d2}}+\frac{1}{R_{d4}} & -\frac{1}{R_{d2}} & 0 & 0 & 0 \\ 0 & 0 & 0 & -\frac{1}{R_{d1}} & -\frac{1}{R_{d2}} & \frac{1}{R_{d1}}+\frac{1}{R_{d2}}+\frac{1}{R_o} & 0 & 0 & 0 \\ 0 & -1 & 1 & 0 & 0 & 0 & 0 & 0 & 0 \\ 0 & 0 & 1 & -1 & 0 & 0 & 0 & 0 & 0 \\ 1 & -1 & 0 & 0 & 0 & 0 & 0 & 0 & 0 \end{bmatrix} \quad (6)$$

Backward Euler (B. Euler) is an implicit numerical analysis technique independent of the step size h. While the method remains stable, selecting a step size that is unnecessarily small significantly increases the simulation time. It is generally enough to define h as smaller than the smallest time constant of the system. In this study, the simulation step size was set to 20nS.

The sequential stages of integrating the Backward Euler method into the MNA framework are demonstrated below.

$$\frac{dX}{dt} = -\frac{G}{C}X(t) + \frac{B}{C}U(t) \quad (7)$$

$$X_{n+1} = X_n + h(-\frac{G}{C}X_{n+1} + \frac{B}{C}U_{n+1}) \quad (8)$$

$$X_{n+1} = K_A \cdot X_n + K_B \cdot U_{n+1} \quad (9)$$

$$K_A = ([C + hG]^{-1} \cdot C) \quad (10)$$

$$K_B = ([C + hG]^{-1} \cdot B \cdot h) \quad (11)$$

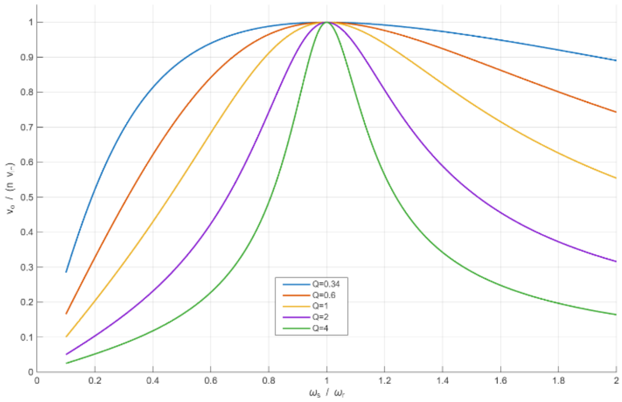

Figure 5. Gain Characteristics for Different Q Values

$$\frac{v_o}{nv_{in}} = \frac{1}{\sqrt{\left(1 + Q^2\left(\frac{\omega_r}{\omega_s} - \frac{\omega_s}{\omega_r}\right)^2\right)}} \quad (12)$$

Equation 7 describes the voltage gain of the resonant circuit. The quality factor (Q) graph in Fig. 5 is calculated by Equation 7. This figure shows us the relationship between the input voltage V_{in} and the output voltage V_{out}.

As illustrated in Fig. 5, the resonant tank exhibits different responses depending on the load conditions. The effect of the load on the normalized gain is examined as a function of the normalized frequency, independent of the transformer characteristics. Based on the expected load conditions, an appropriate quality factor (Q factor) should be selected, and the converter design should be carried out accordingly.

The classification of the load as light or heavy is determined by the load current level. For applications operating under light-load conditions, the blue curve shown in Fig. 5, corresponding to a quality factor of Q=0.34, is selected. This choice ensures stable resonant operation and favorable gain characteristics under the intended operating conditions.

For the subsequent analysis, the calculation of the required circuit parameters begins with the selection of the switching frequency. Once the operating frequency is determined, the resonant tank components can be designed accordingly. When a switching frequency of 135kHz and resonance inductance of 100µH are selected, either the inductance or capacitance value can be predefined, and the remaining parameter can then be calculated using the resonant frequency relationship given in Equations 8 and 9.

Selecting switching and resonant frequencies below 150 kHz—the starting threshold for EMC testing—serves to minimize potential EMI and RFI problems at the initial design stage. For resonant converters, a switching frequency range between 100 kHz and 150 kHz provides an optimal balance regarding the dimensions and efficiency of transformers and other winding components. Subsequently, the values of the resonant tank elements, C_r and L_r, are calculated based on this selected frequency.

$$135 \cdot 10^3 = \frac{1}{2\pi\sqrt{100.10^{-3} \cdot C}} \quad (13)$$

$$C \approx 1.39 \cdot 10^{-8} \approx 14nF \quad (14)$$

Alternatively, the resonant tank parameters can be calculated by first selecting the desired quality factor and then determining the equivalent AC load resistance. This approach is expressed by Equation 10, 11, 12 and 13. Due to the light-load operating condition considered in this study, the quality factor is chosen as Q=0.34.

Table 1 Input Parameters

Element	Value
Input Voltage	±500V
Switching Frequency	135 kHz
Duty Cycle	0.45
L_r	100µH
L_{eq}	720µH
$R_{d,min}$	1mΩ
$R_{d,max}$	1MΩ
C_r	14nF
R_o	245Ω
C_o	100µF
n	10
R_{ser}	0.1Ω
Output Voltage	490V

$$I_o = \frac{V_o}{R_o} = \frac{490}{245} = 2\,A \quad (15)$$

$$R_{ac} = \frac{8}{\pi^2}\frac{V_o}{I_o} = \frac{8}{3.14^2} \cdot \frac{490}{2} = 246\,\Omega \quad (16)$$

$$C_r = \frac{1}{2\pi f_r R_{ac} Q} = \frac{1}{2\pi \cdot 135 \cdot 10^3 \cdot 246 \cdot 0.34} \cong 14nF \quad (17)$$

$$L_r = \frac{1}{(2\pi f_r)^2 C_r} \quad (18)$$

$$L_r = \frac{1}{(2\pi \cdot 135 \cdot 10^3)^2 \cdot 14 \cdot 10^{-9}} \cong 100\mu H \quad (19)$$

3.1. Simulation-Based Results

The simulation results obtained using the Backward Euler (B. Euler) method, based on the derived MNA matrices and circuit parameters, are presented in Figs. 6–11. These results are used to evaluate the dynamic behavior and switching characteristics of the proposed ZCS push-pull converter.

The graphs of the resonant circuit exhibiting ZCS characteristics can be seen in Figures 7 and 8.

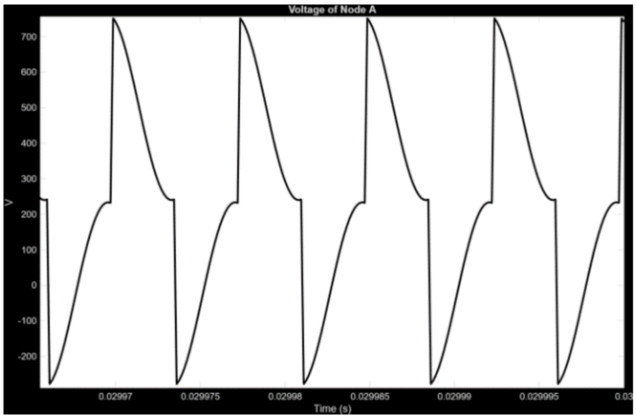

Figure 6. Secondary Side Voltage at Node A

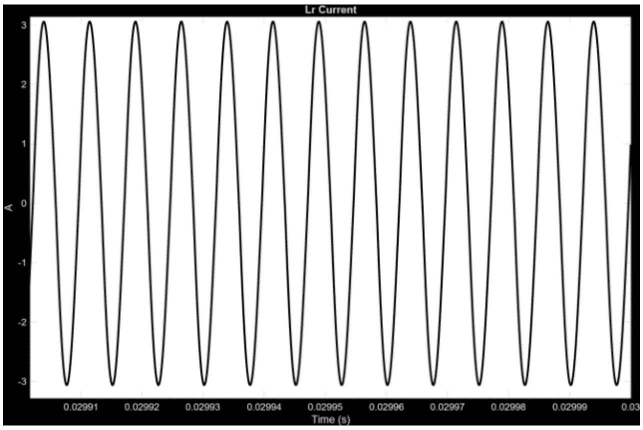

Figure 7. Resonant Inductor Current

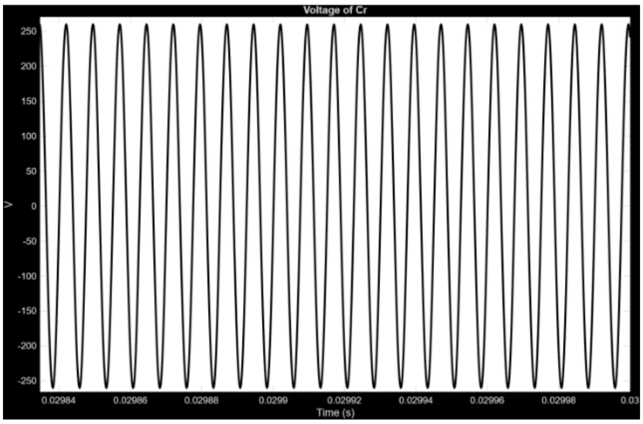

Figure 8. Resonant Capacitor Voltage

The sinusoidal current and voltage waveforms observed across the Lr and Cr components confirm that resonance is successfully achieved. The resulting waveforms demonstrate that the resonant interaction between these elements effectively enables soft-switching conditions within the converter. The sinusoidal waveforms generated by the interaction of the resonant components are subsequently rectified by the output diodes, resulting in full-wave rectification, as illustrated in Fig. 9

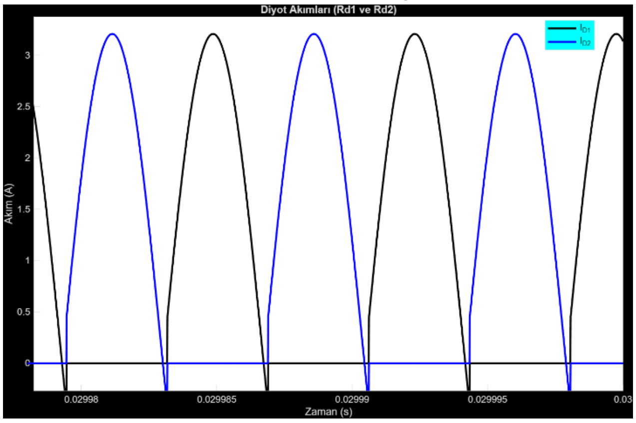

Figure 9. Full-Wave Rectification by Diodes D1 and D2

Figure 9 presents the current waveforms through diodes D1 and D2. It is observed that current commutation occurs at zero-crossing instants. Since the diodes are switched when the current is zero, zero-current switching (ZCS) operation is achieved. This behavior represents a critical feature of the proposed topology and directly contributes to reduced switching losses and improved efficiency.

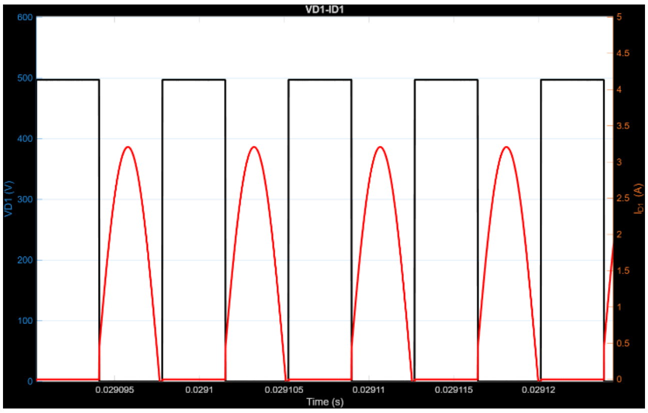

Figure 10. Current-Voltage Characteristics of Diode D1

The voltage and current waveforms of diode D2 are presented in greater detail in Fig. 10. The absence of abrupt current and voltage transients further confirms the effectiveness of the ZCS mechanism in mitigating switching stress.

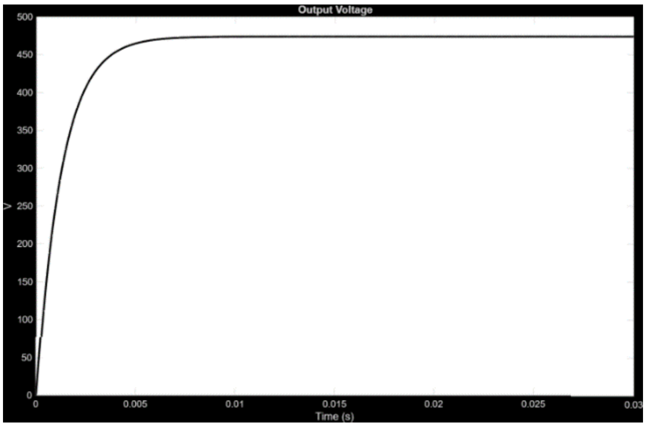

Figure 11. Output Voltage Waveform

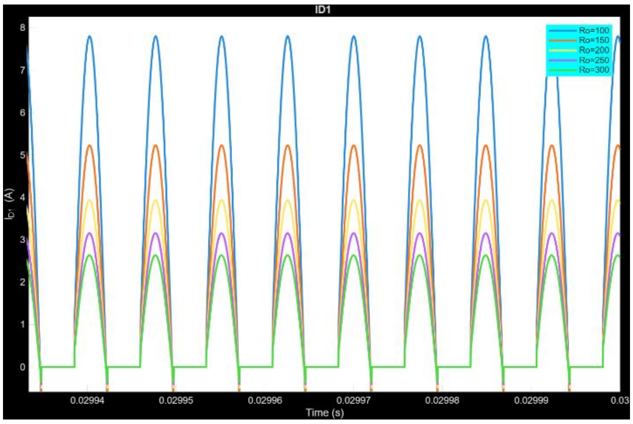

Figure 12. Half-Wave Rectification Under Different Loads

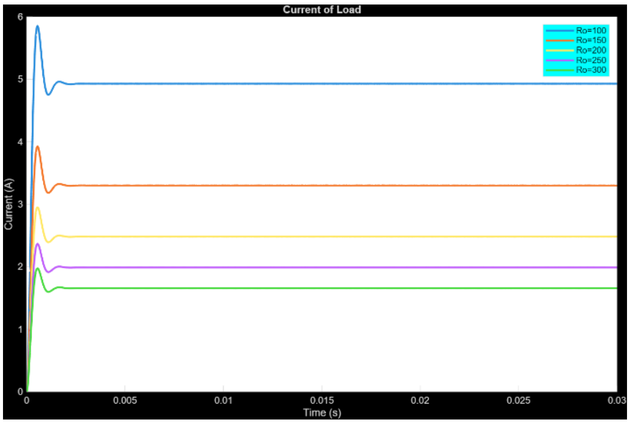

Figure 13. Output Currents Under Different Loads

In Figures 12 and 13, it is observed that the output current and the sinusoidal waveform maintain their structural integrity across different load conditions, demonstrating that the system operates stably as a wide-range load system.

4. Conclusions

In this study, a resonant push-pull DC–DC converter is analyzed using the Modified Nodal Analysis (MNA) technique. The simulation results demonstrate that the proposed topology achieves zero-current switching (ZCS) operation at the output diodes, as evidenced by the current and voltage waveforms presented in Figs. 9 and 10. The sinusoidal current and voltage waveforms generated within the resonant elements enable soft-switching behavior, thereby significantly reducing switching losses.

Furthermore, the implementation of soft-switching resonant operation not only improves converter efficiency but also mitigates thermal stress on the switching devices. As a result, the cooling requirements of the power electronic components can be reduced, leading to lower system cost and enhanced reliability. The presented MNA-based analysis framework provides an effective and systematic approach for modelling and evaluating resonant push-pull converter topologies and can be extended to the analysis of other soft-switching power converter structures.

The applicability of this method serves as a foundation for the analysis and simulation of other circuit topologies. Analyzing resonant circuits through such techniques is significant not only for contributing to the academic body of knowledge but also for minimizing prototype development costs.

Conflict of Interest

The authors of this article declare that the materials and methods used in this study do not require ethical committee permission and/or legal-special permission.

Declaration of Ethical Standards

The author of this article declares that the materials and methods used in this study do not require ethical committee permission and/or legal-special permission.

References

[1] Kazimierczuk MK. Pulse-width modulated DC-DC power converters. 2nd ed. Hoboken: Wiley; 2015.

[2] Erickson RW, Maksimovic D. Fundamentals of power electronics. 2nd ed. New York: Springer; 2001.

[3] Kassakian JG, Schlecht MF, Verghese GC. Principles of power electronics. Reading (MA): Addison-Wesley; 1991.

[4] Baig MJ, Singh RK. A soft-switched ZVS-ZCS boost converter design and analysis. In: IEEE 3rd International Conference on Electrical Power and Energy Systems (ICEPES); 2024; Bhopal, India. p. 1-4. Available from: https://doi.org/10.1109/ICEPES60647.2024.10653601

[5] Kumar S, Singh SK. A novel ZVS/ZCS push-pull LC resonant DC-DC converter for energy sources. Energies. 2023;16(6):2892. Available from: https://doi.org/10.3390/en16062892

[6] Mohammed SAQ, Jung J-W. A state-of-the-art review on soft-switching techniques for DC-DC, DC-AC, AC-DC, and AC-AC power converters. IEEE Transactions on Industrial Informatics. 2021;17(10):6569-6582. Available from: https://doi.org/10.1109/TII.2021.3058218

[7] Xiao H, Wu Q, Xi H. Analysis and design of a wide range ZVS/ZCS Push-pull DC/DC converter with voltage-clamped. IET Power Electronics. 2022;15:422-433. Available from: https://doi.org/10.1049/pel2.12242

[8] Pahlevaninezhad M, Jain PK, Bakhshai A. Zero-voltage switching resonant converters: A review. IEEE Transactions on Power Electronics. 2014;29(2):765-778.

[9] Assaf J, Menye JS, Camara MB, Guilbert D, Dakyo B. Power converter topologies for heat pumps powered by renewable energy sources: A literature review.

Electronics. 2024;13:3965. Available from: https://doi.org/10.3390/electronics13193965

[10] Kulkarni C, Joshi P. Modeling push-pull converter for efficiency improvement. Electronics. 2022;11(17):2713. Available from: https://doi.org/10.3390/electronics11172713

[11] Mosallam HA, Badran EA. A systematic review of DC-DC converter technologies: Traditional, bidirectional, and impedance-source topologies. Discover Electronics. 2026;3:16. Available from: https://doi.org/10.1007/s44291-026-00168-0

[12] Huang Z, Zhu S, Feng W, Li M, Shi S, Lai J. A flyback converter with a simple passive circuit for improving power efficiency. Energies. 2024;17(18):4729. Available from: https://doi.org/10.3390/en17184729

[13] Tanji Y, Kamei H. Behavioral modeling of class E amplifiers based on modified nodal analysis formulation. In: IEEE 10th International Conference on Power Electronics and Drive Systems (PEDS); 2013; Kitakyushu, Japan. p. 6-11. Available from: https://doi.org/10.1109/PEDS.2013.6526979

[14] Nguyen CV, Huynh KD, Hoang XH, Ngo DP, Ho TP, Le AN. Improving the efficiency of push-pull converter using resonance. In: International Symposium on Electrical and Electronics Engineering (ISEE); 2025; Ho Chi Minh, Vietnam. p. 143-148. Available from: https://doi.org/10.1109/ISEE68370.2025.11223502

[15] Ho C-W, Ruehli AE, Brennan PA. The modified nodal approach to network analysis. IEEE Transactions on Circuits and Systems. 1975;22(6):504-509. Available from: https://doi.org/10.1109/TCS.1975.1084079

[16] Voyer N, Nakabayashi A, Kondo R. Fast circuit simulation of linear electronic circuits using modified nodal analysis. In: IEEE Energy Conversion Congress and Exposition (ECCE); 2024; Phoenix, AZ, USA. p. 3825-3832. Available from: https://doi.org/10.1109/ECCE55643.2024.10860273

[17] Voyer N, Nakabayashi A, Kondo R. Fast circuit simulation of power electronic circuits using modified nodal analysis. IEEE Transactions on Power Electronics. 2026;41(2):1866-1878. Available from: https://doi.org/10.1109/TPEL.2025.3604213

[18] Tong WPQ, Muhammad Ramadan BMS, Logenthiran T, Naayagi RT, Woo WL, Phan V-T. High-performance CLL resonant multi-channel LED driver for lighting application. In: IEEE 4th Southern Power Electronics Conference (SPEC); 2018; Singapore. p. 1-6. Available from: https://doi.org/10.1109/SPEC.2018.8635959

[19] Rashid MH, Hui SY, Chung HSH, Madichetty S, Shanthi Kumar NB, Mohan Krishna B. Resonant and soft-switching converters. In: Rashid MH, editor. Power electronics handbook. 5th ed. Oxford: Butterworth-Heinemann; 2024. p. 345-405. Available from: https://doi.org/10.1016/B978-0-12-811407-0.00012-X

[20] Lin B-R. Resonant converter with soft switching and wide voltage operation. Energies. 2019;12(18):3479. Available from: https://doi.org/10.3390/en12183479